Abrasive Wear Resistance, Mechanical Behaviour, Water Transport Phenomena and Biocorrosion of Epoxy/Femora Biocomposites

J.L. Olajide[a,c], I.O. Oladele[a,d], O.J. Odeyemi[a], S.O. Babarinsa[a,b]

[a]*Department of Metallurgical and Materials Engineering, Federal University of Technology, Akure, Nigeria,*
[b]*Department of Mechanical Engineering, Nigerian Defence Academy, Kaduna, Nigeria,*
[c]*Division of Computational Materials Science and Prototype Engineering Development, Quantum Simutech Enterprise, Ilorin, Nigeria,*
[d]*African Materials Science and Engineering Network (AMSEN), A Carnegie-IAS (RISE) Network, FUTA Node, Nigeria.*

Corresponding author:

J.L. Olajide
Division of Computational Materials Science and Prototype Engineering Development, Quantum Simutech Enterprise, Ilorin, Nigeria.
E-mail: jimmylolu@gmail.com

A B S T R A C T

Of late, some biological wastes have proven to be reliable candidates in promoting the economic viability of developing polymeric composites. However, the field-proven reliability prediction of such materials during service life requires extensive characterization. In this research, the influence of 75 μm bovine femur ash subjected to two-step calcination process on spectroscopic, wear, mechanical, water absorbent and biocorrosive properties of epoxy/femur waste biocomposites was investigated. The test materials were developed via open mould casting and subjected to preferred characterizations apropos of the abovementioned properties. Elemental constituents of the biocomposites and the ash were determined by energy dispersive x-ray spectroscopy with scanning electron microscopy and x-ray fluorescence spectroscopy, respectively. The investigated properties were studied dependent on predetermined volume fractions of the ash in epoxy matrix. Observations from the experimental results revealed that properties' enhancement was not specific to either low or high volume fraction of the ash in epoxy. Different properties were enhanced at different volume fractions of the ash. Nonetheless, one biocomposite approaching intermediate volume faction of the ash used, exhibited optimum combination of the investigated properties. This is a clear indication that bovine femur waste can be successfully exploited for engineering applications, especially in the areas of materials development.

1. INTRODUCTION

Today, judging by the voluminous nevertheless unexhausted number of publications on Bio-based Filler-reinforced Polymer Matrix Composites (BFPMCs), it is relatively evident that this approach of materials development has preeminently stimulated the interest of

researchers [1-5]. This tremendous interest could be predominantly credited to the broad-spectrum advantage conferred on PMCs by bio-based fillers. Some of their peculiar advantages include environmental friendliness, excellent thermal stability, high wear resistance, high modulus of elasticity, relative abundance, commercial viability and ease of processing [3,4].

In consequence, studies have revealed some of the BFPMCs to have improved biomedical, thermal, tribological and mechanical properties. In one study, Nithya and Sundaram reported the improved biomedical characteristics of ciprofloxacin-loaded polycaprolactone nanocomposite film filled with eggshell-based hydroxyapatite (HAP) [2]. Adeosun *et al.,* in their work reported the positive influence of Snail Shell Ash (SSA) on the glass transition and melting temperatures of unsaturated polyester composites [3]. Asuke *et al.,* also documented a significant enhancement in the wear properties of polypropylene composites filled with micro-sized calcined Bovine Bone Ash (BBA) [4]. Another investigation conducted by Oladele *et al.,* similarly revealed micro-sized SSA to be effective in enhancing wear resistance and mechanical behaviour of epoxy biocomposites [5].

Furthermore, the possibility of synthesizing the biomedically useful product "HAP" from avian eggshells, dead mammalian bones and mollusk shells has facilitated the development of novel PMCs for orthopaedic and maxillofacial applications [2,6,7]. Nonetheless, of interest to the present study is the engineering exploitation of Bovine Femur Wastes (BFW) for BFPMCs development.

BFW are annually generated in ample quantities by slaughterhouses worldwide. Presently, the manufacturers of porcelains are the largest consumers of Bovine Bone Wastes (BBW) [8]. However, in the past, BBW used to find major applications in the biomedical and agricultural sectors, notably as collagen source, organic fertilizers and bone meal for livestock, respectively [9-11]. Consequently, the epidemic of the foot-and-mouth and bovine spongiform encephalopathy diseases culminated in a radical decline from the biomedical and agricultural exploitations of BBW. The foregoing occurrence was dependent on research findings that featured BBW as potential vectors of the

pathogens responsible for the transmittance of these diseases to humans and animals [12].

At the moment, the unsafe disposal of BBW in a country like Nigeria where porcelains are seldom manufactured has become an environmentally threatening issue that requires immediate action [13]. Hence, the pressing need to find alternative ways to exploit BBW productively in Nigeria has become alarmingly crucial.

It is in the light of effectively surmounting the foregoing problem that some researchers began investigating the suitability and efficiency of using BBW to improve some selected properties of PMCs. Agunsoye *et al.,* have reported improved tensile strength and wear resistance of BBA-filled recycled low density polyethylene composites [14]. Correspondingly, another study by Afolabi *et al.,* revealed improved mechanical behaviour and thermal stability of epoxy resin filled with micro-sized BBA [15].

However, most of these research findings are limited to the influence of BBA on the mechanical behaviour of PMCs. The present study focused on microstructural, spectroscopic, mechanical, wear resistant, water absorbent and biocorrosive properties of epoxy biocomposites filled with calcined Bovine Femur Ash (BFA).

Epoxy resin owing to its attractive properties presents polymer scientists and engineers with versatile areas of applications. In the electronic industries, by virtue of its excellent dielectric and thermal properties, it is the primary material of choice for the manufacture of Printed Circuit Boards (PCBs) and electronic components' encapsulants. Its superior adhesive strength has also made it very useful as sealant for joints and gaskets in the aeronautical industries, as binder in cements and mortars, and as solidifying agent for sandy oil rigs. Its excellent combination of wear resistance, adhesive strength and glossy appearance qualifies it as primer paint in the automobile industries and as coatings for walls, floors, statues and household furniture [16,17]. Other notable applications of epoxy are seen in flooring panels, aircraft wings, lightweight bicycle frames, golf clubs, snowboards and racing cars. In addition, its low shrinkage and ability to adhere to a variety of substrates has rendered it one of the most exploited polymers

as matrix for both natural and synthetic fillers/fibres [5].

Nevertheless, maintaining the economic viability of developing BFPMCs in the absence of filler and/or matrix surface modifications often facilitates the time-dependent susceptibility of the composites to water/moisture absorption and environmental degradation. Such undesirable occurrence practically manifests in mechanical, dimensional and chemical properties' degradation in the composites [18].

In the present study, the optimum filler content of unmodified 75 μm calcined BFA required to enhance the structural integrity, wear resistance, low moisture uptake and biocorrosion resistance of epoxy resin was investigated.

2. MATERIALS AND METHODS

2.1 Materials

The basic materials used in this study were Bisphenol A diglycidyl ether epoxy resin (DGEBA commercial grade), diethylene triamine (DETA) curative and Dead Bovine Femurs (DBF). The epoxy resin and the amine curative were sourced and procured from Orkila Chemicals, Ikeja, Lagos State, Nigeria and the DBF were sourced and acquired from slaughterhouses in Akure, Ondo State, Nigeria. The ages of the bovines from which the DBF were obtained were 3 years ±6 months.

2.2 Methods

Preparation of the BFA

The as-received DBF from slaughterhouses were thoroughly scrubbed with synthetic polymeric sponge and rinsed under flowing deionized tap water. This was ensued by sun-drying the DBF at 28 ±5 °C for 14 days. Afterwards, a two-step calcination process was carried out on the sieved powder inside a muffle furnace preheated at 950 °C. For the first and second steps of the calcination process, the powder was heated at 950 °C for 1 hour and 1100 °C for 3 hours, respectively. Subsequently, the dried DBF were transferred into a pulverizing machine to reduce them into powder and this was ensued by sieving the resultant powder through a sieve mesh size of

75 μm. The resultant BFA was then taken to the laboratory for X-ray Fluorescence Spectroscopic (XRF) analysis to determine its elemental constituents. A schematic illustration of the experimental procedure is presented in Fig. 1.
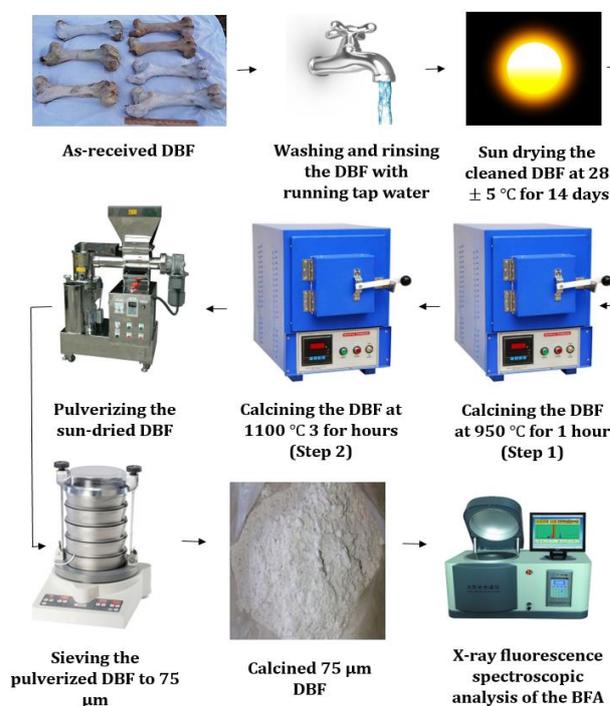

Fig. 1. Schematic illustration of the experimental procedure used to prepare the BFA.

Development of the Epoxy /BFA Biocomposites (EBFABs)

The EBFABs test samples were developed via open mould casting technique with predetermined wt.% BFA of 2, 4, 6, 8, 10, 15 and 20, respectively. Homogeneous mixture of the epoxy resin, the amine curative and the BFA for each test sample was achieved by mechanically mixing the composition for 2 minutes. The homogeneous mixtures were thereafter introduced into respective moulds designed for each property to be investigated and allowed to cure in air. Subsequently, the developed EBFABs and the Neat Epoxy (NE) were transferred to the material testing laboratory for preferred characterizations.

Wear Test

The wear test was conducted in compliance with Taber Wear test standard D4060-14 [19]. The test samples with disc-shaped geometries of 100 mm diameter and thickness of 6.35 mm were mounted to a turntable platform that rotates on a vertical

axis at a fixed speed of 60 rpm. The turntable has dual abrading arms that are precision balanced. Each arm was loaded for 250 g pressure against the test samples and lowered onto the specimen surface. Characteristic rub-wear action is produced by contact of the test sample against the sliding rotation of the two abrading wheels. As the turntable rotates, the wheels are driven by the sample in opposite directions about a horizontal axis displaced tangentially from the axis of the sample. One abrading wheel robs the specimen outward toward the periphery and the other inward toward the center while a vacuum system removes the debris during the test. The test was conducted for 15 minutes for each test sample. The wheels traverse a complete circle on the specimen surface, revealing abrasion resistance at all angles relative to the weave or grain of the material. The resulting abrasion marks form a pattern of crossed arcs in a circular band that covers an area of approximately 30 cm^2. The weight loss of the materials due to abrasion and their wear indices were evaluated using Equations 1 and 2 respectively. The experiment was carried out at room temperature of 24 ±2 °C. Six repeatability tests were conducted for each biocomposite and their mean values were used in this study to ensure accuracy and reliability of test results.

Weight Loss:

$$L = A - B \qquad (1)$$

Where L –Weight Loss; A –Weight of test sample before abrasion in milligrammes; and B –Weight of test sample after abrasion in milligrammes.

Rate of Wear:

$$I = \frac{(A - B) \times 1000}{C} \ \text{(mg/min)} \qquad (2)$$

where I –Taber Wear Index (TIA); A –Weight of test sample before abrasion in milligrammes; B –Weight of test sample after abrasion in milligrammes; and C –number of test cycles in minutes.

Tensile Test

The tensile test was performed in compliance with ASTM D638-14 test standard [20]. The specimen's overall length, gauge length, width and thickness were 115, 33, 10 and 5 ±1 mm, respectively. The tensile test was performed using INSTRON 3382 Floor Model Universal Tester at a fixed crosshead speed of 10 mm/min.

The experiment was carried out at room temperature of 22 ±2 °C. Six repeatability tests were conducted for each biocomposite and their mean values were used in this study to ensure accuracy and reliability of test results.

Flexural Test

Three-point bend test was performed on the test samples in compliance with ASTM D790-15e2 standard [21]. The length, width and thickness of the specimen were 120, 12.7 and 3.2 mm, respectively. Correspondingly, the test was performed on INSTRON 5980-series Floor Model Universal Tester. The machine was operated at a crosshead speed of 0.3 mm/mm and at a specific strain rate of 10^{-3}/s. The test is stopped when the specimen reaches 5 % deflection or breaks before 5 % deflection. The experiment was carried out at room temperature of 22 ±2 °C. Six repeatability tests were conducted for each biocomposite and their mean values were used in this study to ensure accuracy and reliability of test results.

Tensile Impact Test

In the present research, the impact test study was as well used as the criterion to establish the toughness of the developed biocomposites. The tensile impact test was adopted for this research.

The test was carried out on a manual impact testing machine in compliance with ASTM D1822 test standard [22]. The dimension of the test sample notched 2 mm on each side was 80 x 11 x 3 mm. Each of the notched sample was loaded into the arm of the testing machine. The arm was released to break the sample while the breaking load was manually recorded from the machine's display screen for result. The experiment was carried out at room temperature of 24 ±2 °C. Six repeatability tests were conducted for each biocomposite and their mean values were used in this study to ensure accuracy and reliability of test results. The impact strength in kJm^{-2} of the test samples was calculated from their evaluated energy absorbed using Equation 3.

$$Impact\ Strength = \frac{E_{abs}}{(W - n_s) \times L} \qquad (3)$$

where E_{abs} –Energy Absorbed by the sample in (kJ); W –Width of test sample in (m); n_s –Notched section in (m); and L –Thickness of test sample in (m).

Water Absorption Test by Immersion

This was test was conducted in compliance with ASTM D570-98 test standard [23]. Standard sized test samples (same as un-notched impact test samples) were conditioned to constant mass, M_0 at 50 °C and stored in a desiccator prior to the testing. After immersion in deionized water for 24 hours at a room temperature of 22 ±2 °C, the test samples were removed from the water and surface liquid wiped off using a dry cloth before immediately weighing. A digital scale was used to take the initial and final weights of the test samples to the nearest 0.0001 g. Afterwards, the test samples were returned to the water for continuing exposure. It was ensured that the time out of the medium was minimized to 1 minute for each test sample. The exposure was continued for 7 days and halted when the weight gains from 3 successive measurements differed by less than 1 % of the overall weight gain. In order to define the absorption curve, the values of the weight gain in % at different time intervals was plotted against time of immersion (t).

The kinetics of sorption of the materials was studied through Fickian model of diffusion. For accuracy and reliability of test results, the experimental data were obtained from mean values of five test samples from each composition of the biocomposites. The water % absorption, the diffusion exponent and the diffusion constant of the test samples were evaluated using the expressions in Equations 4, 5 and 6, respectively.

$$Water \% Absorption = \frac{W_t - W_d}{W_d} \qquad (4)$$

where W_t –Weight of test sample at a given immersion time and W_d –Weight of dried test sample.

For the determination of diffusion mechanism and kinetics of sorption, the conventional power-law relations were used for the initial stage of water absorption where $M_{r(t)}/M_\infty < 0.5$:

$$\frac{M_{r(t)}}{M_\infty} = kt^n \qquad (5)$$

$$log \frac{M_{r(t)}}{M_\infty} = \log k + n \log t \qquad (6)$$

Where $M_{r(t)}$ –Relative Mass Uptake at time t; M_∞ –Saturated Mass Uptake; t –time; n –constant that determines the diffusion case; and k –constant related to the structure of the polymer network [24]. The values of n and k were calculated from the slope and intercept of the linear part of the log-log plot of $(M_{r(t)}/M_\infty)$ versus time of immersion (t). The values were drawn from the experimental data.

Biocorrosion Test

The biocorrosion test was done in compliance with ISO 846-1997 test standard [25]. Test samples of known weights and dimension of 0.1mm x 01mm x 0.05mm were buried in the soil for 30 days and exhumed on the 30th days for final weight measurements. The biocorrosive potential of the materials was evaluated via visual examination and measurement of changes in mass. The measurement of changes in mass was calculated using Equation 7.

$$\Delta M = M_2 - M_1 \qquad (7)$$

where ΔM –Change in weight; M_1 –Initial weight of test sample before soil burial process and M_2 –Final weight of test sample after soil burial process.

Scanning Electron Microscopy (SEM)

The fractured surfaces of post-impact test samples were observed with (SEM) JEOL-JSM 6300, 20 kV scanning electron microscope. To make the samples conductive, they were vacuum-coated with a thin film of gold.

Scanning Electron Microscopy with Energy Dispersive X-ray Spectroscopy

Test samples were placed within the vacuum chamber located at the bottom of the scanning electron microscope column (German brand AURIGA, Carl Zeiss 2010 model). An electron source, located at the top of the column, produced electrons that passed through the column and were incident upon the test samples. The electron beam was directed and focused by magnets and lens inside of the scanning electron microscope column as it approached the test samples. The beam swung across the samples causing some of the electrons to be reflected by the test samples and some to be absorbed. Specialized x-ray detectors received these electrons and processed the signal into a usable format. From four spectra examined from each test sample, the closest two spectral details were selected for discussion in the present study.

3. RESULTS AND DISCUSSION

3.1 XRF Spectroscopy Observations

The XRF analysis result of the BFA is presented in Table 1. From the result, Ca was revealed as the principal element which translates to ability of bovine bone to retain some of its inherent properties after thermal decomposition [26].

**Table 1.** XRF Analysis Result for the BFA

Element	Conc. Value wt.%	Conc. Error ±
Ca	55.75	3.80
Zn	20.10	2.10
Fe	16.49	1.04
K	2.12	0.11
Ti	0.55	0.05
Cr	0.07	0.01
Ni	0.01	0.01
Zn	0.09	0.02
Na	1.32	0.21
Mn	2.90	0.50
Cu	1.43	0.20
Mg	0.18	0.30

3.2 SEM-EDS Observations

The SEM-EDS result of the 20 wt.% EBFAB selected as the representative sample for the EBFABs is presented in Figs. 2a and 2b. This result somewhat revealed a fair dispersion of the BFA within the NE matrix.
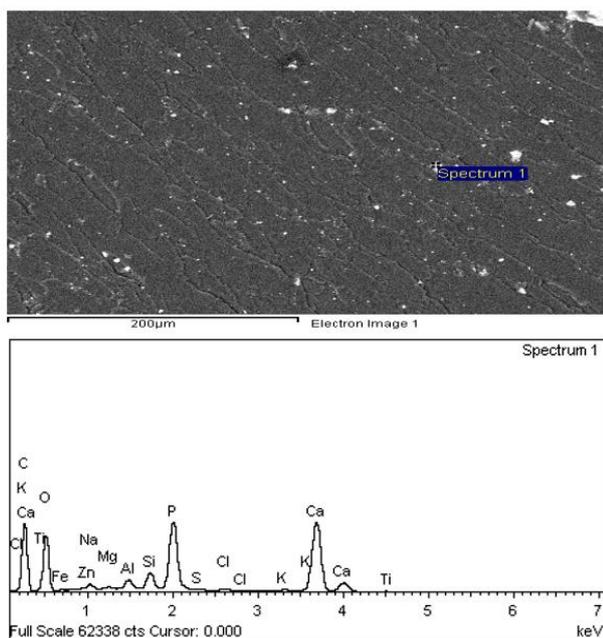
Fig. 2a. SEM-EDS result of the 20 wt.% EBFAB showing Ca, O and P Peaks which translates to high Calcium Phosphate content in the biocomposite.
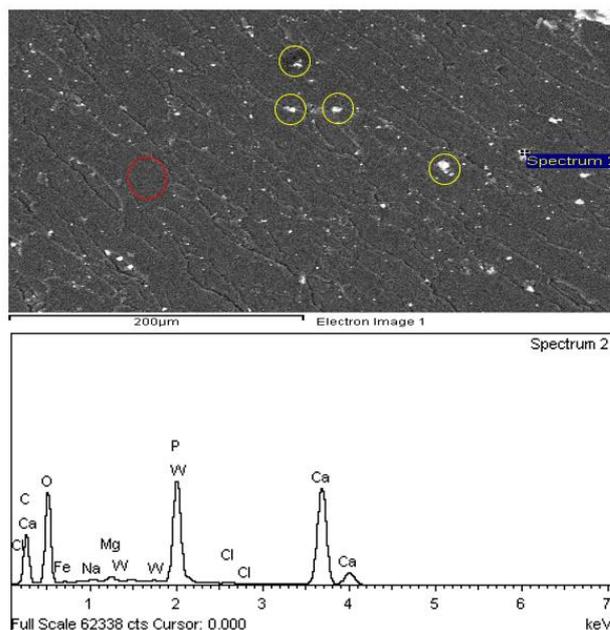
Fig. 2b. SEM-EDS result of the 20 wt.% EBFAB showing BFA particles in enclosed yellow circles and the red circle showing a segment of the NE matrix.

Table 2. Quantitative EDS result of the BFA.

| E	MOS	SEM	STD	MaxV	MinV
C	32.43	7.57	10.71	40.00	24.86
O	37.91	5.05	7.14	42.96	32.86
Na	0.37	0.16	0.22	0.52	0.21
Mg	0.30	0.15	0.21	0.45	0.15
Al	0.39	0.39	0.54	0.77	0.00
Si	0.79	0.79	1.11	1.57	0.00
P	9.84	1.59	2.26	11.43	8.24
S	0.09	0.09	0.12	0.17	0.00
Cl	0.19	0.09	0.12	0.27	0.10
K	0.11	0.11	0.15	0.21	0.00
Ca	16.79	2.16	3.05	18.94	14.63
Ti	0.06	0.06	0.08	0.11	0.00
Fe	0.34	0.03	0.04	0.37	0.31
Zn	0.10	0.10	0.14	0.20	0.00
W	0.34	0.34	0.48	0.68	0.00
*E = Element; MOS = Mean of Spectra; SEM= Standard Error of Mean; STD = Standard Deviation; MaxV = Maximum Value and MinV = Minimum Value					

From Table 2, it can be seen from the EDS result, that the biocomposite contains a substantial amount of calcium phosphate mineral. As obtainable from existing literature, about 70 % of bone consists of Calcium Phosphate mineral in the form of HAP. The chemical formula for HAP is $Ca_5(PO_4)_3(OH)$ [27].

3.3 Abrasive Properties

In Figure 3, the influence of wt.% BFA on the abrasion test results (weight loss and wear indices) of the EBFABs is presented. From the

results, it was observed that the lowest and highest filler contents gave the most significant enhancements.
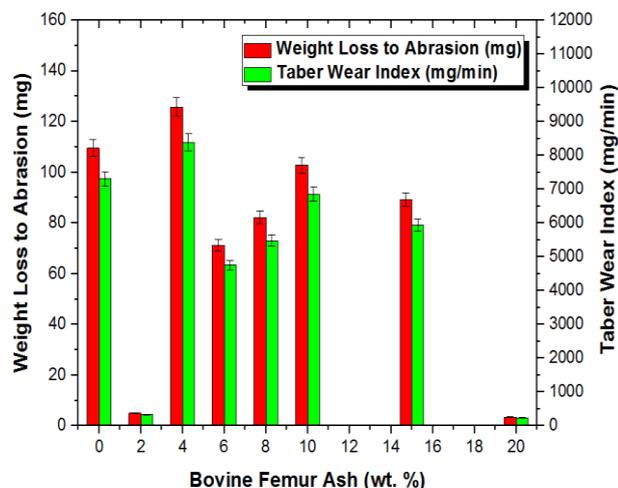
Fig. 3. Variation of Weight Loss to Abrasion and Taber Wear Index with wt.% BFA for the NE and the EBFABs.

This occurrence at the foregoing filler contents can be attributed to increase in asperity of surface topography of the biocomposites and very strong binding energy/strength of interfacial adhesion between the BFA fillers and the epoxy matrix.

It can be said for the 2 wt.% EBFAB, that the epoxy matrix is sufficient enough to render an efficiently supporting parent phase for the BFA fillers. And owing to this effect, the BFA fillers were not easily debonded from the epoxy matrix under abrasive loading but acted as wear resisting agents.

However, for the 20 wt.% EBFAB two other modes of strengthen mechanism based on increasing population of the BFA filler in the epoxy matrix were observed. The first mode was based on direct variation of increasing filler content with filler-matrix compaction while the second mode was based on direct variation of increasing filler content with increased asperity on surface topography of the biocomposite. Some researchers have established these mechanisms to be highly effective in enhancing the wear properties of bio-based ash-filled PMCs [5].

In addition, the inherent bioceramic hard phase associated with BFA and the presence of hard and wear-resistant elements like Tungsten and Silicon in the materials as confirmed by the XRF

analysis result might have contributed to the improvement in wear properties of the biocomposites.

In comparison with the NE and the other EBFABs, the 20 wt.% EBFAB gave the superlative enhancement in wear properties with 3031.4290 and 3031.4286 % reduction in wear index and weight loss to abrasion, respectively.

3.4 Mechanical Properties

Tensile Properties

The variation of Young's Modulus with wt.% BFA for the NE and the EBFABs is presented in Fig. 4. From the result, it was observed that there was a corresponding increase in the Young's Moduli of the EBFABs with increasing filler content in the epoxy matrix until a plateau state was reached at 15 wt.%.
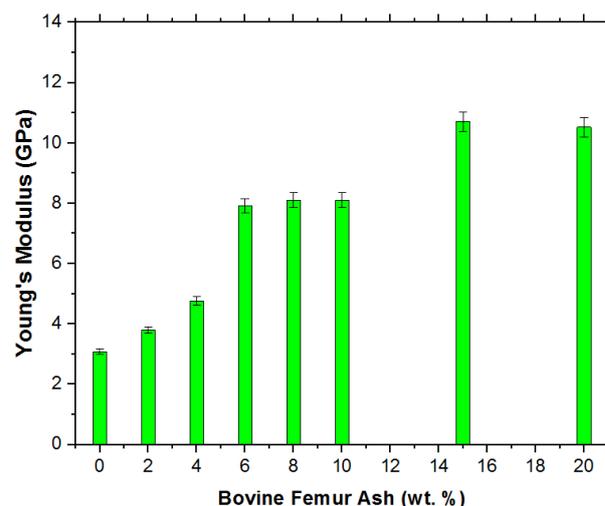
Fig. 4. Variation of Young's Modulus with wt.% BFA for the NE and the EBFABs.

It should be noted that Calcium and Phosphorus are the major constituents of the ash as confirmed by the XRF analysis result. Thus, the ash would behave like calcium phosphate mineral or HAP which is regarded as a bioceramic. Based on reports obtainable from existing literature, the modulus of bovine femur could be as high as 28.4 GPa [28].

In comparison with the NE and the EBFABs, the superlative enhancement in this property was given by the 15 wt.% EBFAB with a 248.26 % enhancement. Researchers have explained that the primary strengthening mechanism in play

here is the transfer of stiffness from the more rigid fillers to the ductile polymer matrix. They explained that this stiffness invariably increases with increasing volume fraction of the fillers in the matrix until a plateau state is reach where the influence of fillers either becomes insignificant or unfavorable [5]. The findings of this research are in conformity with their explanations.
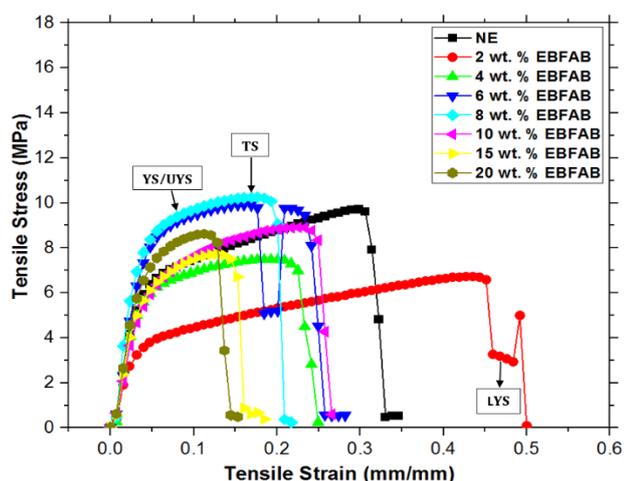

Fig. 5. Stress-Strain curves for the NE and the EBFABs.

According to materials scientists and engineers, the stress-strain curve of a material can be used to explain its response to applied static load or a load that changes relatively slowly with time provided the load is uniformly distributed over its cross section or surface member [29]. In the case of tensile loading, such a curve is sufficient to give detailed information about the tensile strength (TS), yield strength (YS) and strain to fracture of the material.

In Fig. 5, the stress-strain curves for the NE and the EBFABs are presented. From the result, it was observed that at low filler contents of 2-4 wt.% BFA in the epoxy matrix, the tensile and yield strengths were not enhanced. However, the 2 wt.% EBFAB exhibited the superlative ductility/strain to fracture in comparison with the NE and the EBFABs. Correspondingly, the NE outperformed all the EBFABs from 4-20 wt.% filler loadings in terms of strain to failure. This occurrence can be credited to the highly deformable amorphous regions of the NE and the 2 wt.% EBFAB i.e. effect of fillers on polymer chain mobility at this filler content is somewhat negligible. In addition, the positive influence of the high strength of matrix-filler interfacial adhesion discussed under the wear properties of the 2 wt.% EBFAB is also responsible for this significant enhancement in its ductility.

Observations also revealed that the 20 wt.% EBFAB underwent the least plastic deformation before fracture. In fact, it failed in a quasi-brittle manner which is a function of its high stiffness. Nonetheless, the EBFABs retained appreciable ductility until a BFA filler content of 10 wt.%. Hence composites with filler contents less than 10 wt.% delivered the BFA in a fracture tough condition.

With respect to tensile and yield strengths, the superlative performance was given by the 8 wt.% EBFAB. This significant improvement is also dependent on the strength of interfacial adhesion between the filler and the matrix which usually deteriorates with increasing filler content. However, the influence of the strength of interfacial adhesion between the filler and matrix is more pronounced on the tensile strength than on yield strength. Owing to this fact and substantiated by observations from the result, while the positive influence of the BFA on tensile strength started declining at 10 wt.% filler content, its positive influence on yield strength still continued till 20 wt.%. The significant enhancement in these strengths as explained by researchers is a function of efficient load transfer between the composite phases, realized via shear stress induced in the interface region [5].

On an interesting account, two of the EBFABs exhibited very unusual characteristics. The 2 and 6 wt.% EBFABs exhibited both upper and lower yield points (UYS and LYS) which translates to the abilities of these materials to undergo strain hardening after excessive plastic deformation. This behaviour has explained by Ito *et al.*, is due to the transient behaviour of polymers at a given moderate strain rate associated with mechanical heterogeneity expressed as a distribution of relaxation time [30]. For the 6 wt.% EBFAB, the UYS and the LYS were observed at 0.1 and 0.18 strains respectively. Likewise, for the 2 wt.% EBFAB, the UYS and the LYS were observed at 0.1 and 0.46 strains, respectively.

Flexural Properties

Figure 6 shows the variations of flexural strength at peak and flexural strength at yield with filler content for the NE and the EBFABs. From the result, a similar trend observed with variation of tensile strength with wt.% BFA was also observed.

The significant enhancements were observed as the filler content approached intermediate filler loading i.e. 10 wt.% filler loading.
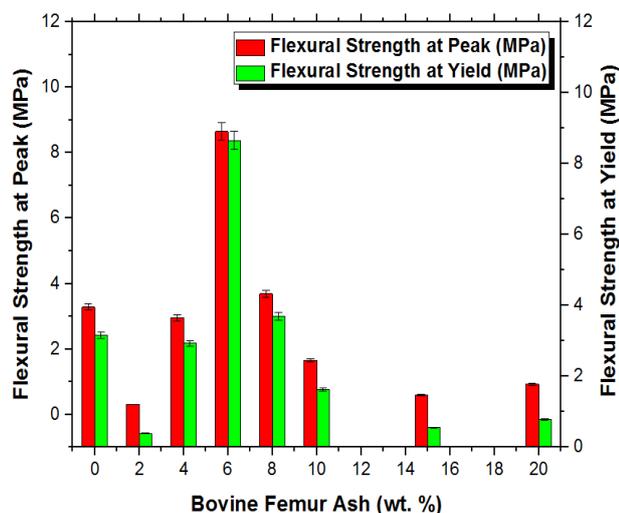

Fig. 6. Variation of Flexural Strength at Peak and Flexural Strength at Yield with wt.% BFA for the NE and the EBFABs.

In comparison with the NE and the EBFABs, the superlative enhancement in these properties was given by the 6 wt.% EBFAB. The flexural strength at peak of this composite was improved by 163.38 % while its flexural strength at yield was improved by 173.49 %. From the result, it was also observed that there was no significant difference between the flexural strengths at peak and at yield of the all materials irrespective of filler content. The mechanism of enhancement in play here is quite different from the one under tensile loading, it is dependent on the load bearing capacity of the fillers and not their functions as stress raisers [5]. And this explains why there is a difference in the trend of results of the flexural and tensile strengths at peak of the NE and the EBFABs. Another reason for this dissimilar trend is the localized nature of flexural test that does not allow uniform resistance of the material to deformation under the application of external load. However, the results of the flexural and tensile strengths at yield of the materials have a relatively similar pattern.

Impact Resistance and Energy Absorption Performance

In Fig. 7 the variations of impact energy and impact strength for the NE and EBFABs are presented. The result revealed that irrespective of wt.% BFA in the epoxy matrix, these properties were not enhanced.
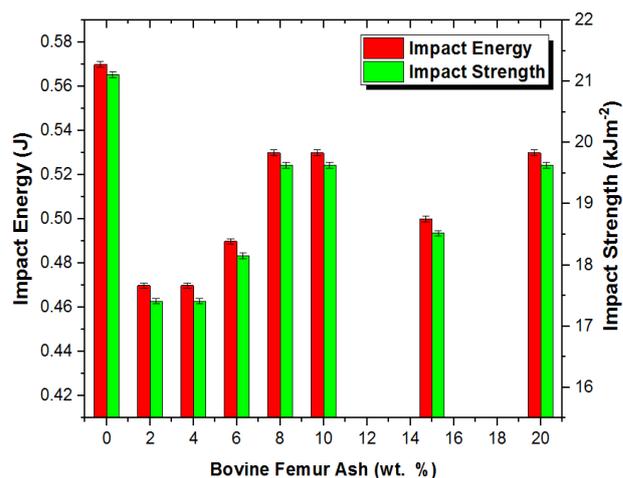
**Fig. 7.** Variation of Impact Energy and Impact Strength with wt.% BFA for the NE and the EBFABs.

However, contrary to most previous research findings, the negative influence of the BFA on the impact resistance and energy absorption performance of composites was more pronounced at low filler contents.

This interesting phenomenon observed at high filler contents could be due to the increase in the contents of elements like Tungsten and Silicon (constituents of BFA) acting as toughening agents in the biocomposites. Nonetheless, the overall reduction in the impact properties of the biocomposites is as a result of BFA-induced brittleness and unfavourable interparticle distance associated with micro-sized fillers [5]. It is believed in this study that the interparticle distance was long enough to allow the matrix ligament lie in the plane strain state where post yield deformation of the epoxy matrix becomes difficult. Also, the induced brittleness would result in limited abilities of the materials to absorb energy by localized shear yield deformation. Hence, the materials cannot be toughened irrespective of filler-matrix mixture homogeneity.

Moreover, epoxy is generally characterized with low toughness and rubbery/nano-sized fillers are the best fits for enhancing its toughness [31]. The BFA used in the present study has no rubbery characteristics, in fact, they are ceramic in nature.

3.5 Morphological Observations

The SEM micrographs of the 6 and 20 wt.% EBFABs selected as the representative samples for the biocomposites are presented in Fig. 8.
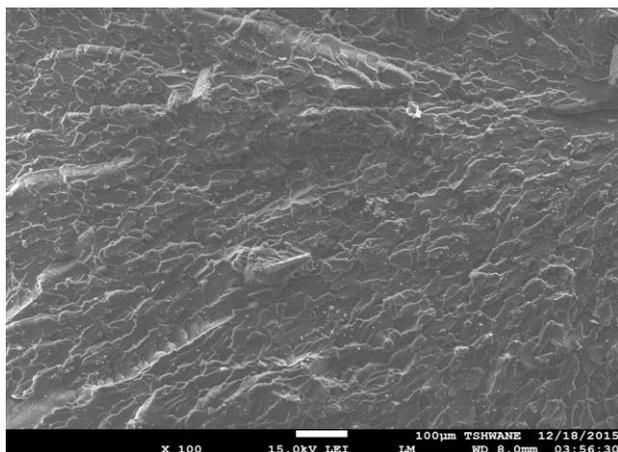
Fig. 8a. SEM fractured surface image of the 6 wt.% EBFAB.
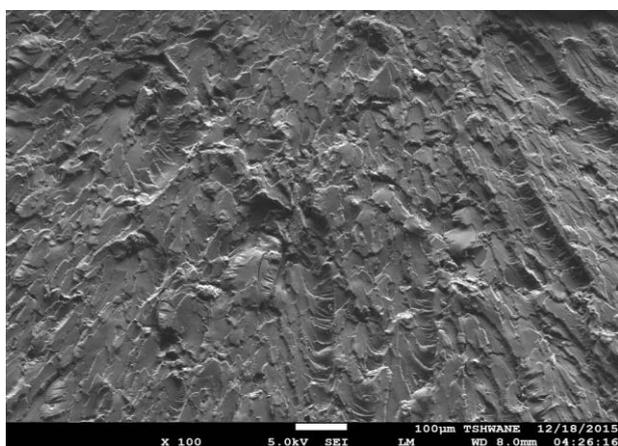
Fig. 8b. SEM fractured surface image of the 20 wt.% EBFAB.

In Fig. 8a, an even distribution of the BFA within the epoxy matrix can be observed. This is expected as filler-filler interaction is significantly limited at this filler content (6 wt.%). This is an indication that formation of filler agglomerates is very difficult as individual fillers are firmly bonded to the epoxy matrix. The absence of agglomerates prevents formation of micro-voids which results in crazes.

The micro-mechanism of failure in particulate filled PMCs is dependent on debonding of the particles from the matrix via dewetting and shear yielding of the matrix via crazing [5]. In the present study, the combination of the even dispersion of the filler and the high strength of interfacial adhesion allow the material to undergo excessive post-yield deformation before shear yielding of the epoxy matrix becomes predominant i.e. it is a ductile mode of failure. In the ductile mode, the epoxy matrix is not restricted in its ability to stretch to support a

load and therefore would be expected to provide greater strength.

Furthermore, at low filler content, the fillers act as effective barriers to dislocation motion by pinning and blocking advancing crack tips, thereby slowing down crack propagation through the material. These observations are supported by the rough fractured surfaces of the material observed in Fig. 8a, high strength and appreciable strain to fracture observed under the tensile properties result.

However, at high filler content as in the case of the 20 wt.% EBFAB the mode of failure is quite different. In Fig. 8b, large smooth surface grooves are observed which translates to sites of debonded fillers/filler agglomerates. At this filler content, formation of isolated agglomerates and localized network of agglomerates becomes very easy as filler-filler interaction prevails over filler-matrix interaction. It is important to note that agglomerates unlike individual fillers do not impede advancing crack fronts but serve as crack initiation sites.

Moreover, weak interfaces within the composites highly promotes agglomerates debonding and debonding which leaves large voids within the material system. So, in response to applied load, the mechanisms of void formation, coalescence of voids and crazing becomes effective and this result in very easy crack initiation and rapid crack propagation in the material. Hence, a transition from ductile to quasi-brittle failure mode occurs. The resultant mode of failure is accompanied by low strain to failure as observed in the stress-strain curve of the composites.

3.6 Water Transport Phenomena

Fundamentally, it is essential for polymer scientists and engineers to know the maximum water uptake of a polymeric material that would not result in hydrolytic degrdation of the material's properties during its service life. In the present study, the rate of water absorption and kinetics of sorption of the EBFABs are presented.

Rate of Water Absorption

The plot of water absorption curve as a function of wt.% gain versus time of immersion in hours for the NE and the EBFABs is presented in Fig. 8.
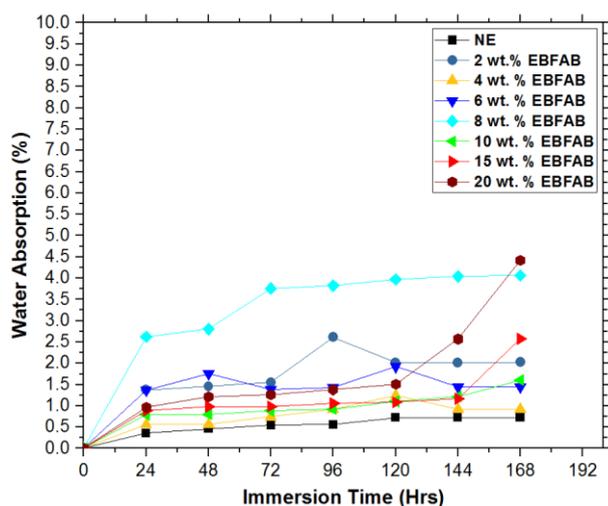
Fig. 9. Plot of water % absorption against immersion time for the NE and the EBFABs.

From the result, it can be seen that, at low filler contents ranging from 2-6 wt.%, the absorption curves for the test samples are somewhat similar (desorption occurs after saturation). Correspondingly, at high filler contents ranging from 10-20 wt.%, the absorption curves have the same pattern (absorption continues after saturation).

Aside from the 6 wt. % EBFAB, all the samples including the NE exhibited a corresponding increase in water absorption with increasing time of immersion which translates to a linear relationship between these two parameters. This linearity existed till 120th hour for nearly all the samples which is also the time where saturation mass uptake began for most of the samples.

Although, the 20 wt.% EBFAB gave maximum water absorption of 4 % at cessation time of the experiment i.e. 168th hour, the 8 wt.% EBFAB had the highest progressive water absorption till 144th hour and the NE exhibited the least progressive water absorption with increasing time of immersion.

There is no regular trend in the water absorption of the EBFABs with increasing filler contents which may be due to the variations in the concentrations of the hydrophilic contents of the BFA in each EBFAB. BFA is majorly composed of HAP which is hydrophilic in nature owing to its (OH) ending which has a strong affinity for water. This explains why the EBFABs absorb more water than the hydrophobic NE. Although, it is expected that the biocomposite

with highest content of BFA should absorb most water, the effect of phosphate concentration, microvoids and weak interfaces within the biocomposites also facilitates diffusion of water into them [24]. On the contrary, reduced water affinity and water desorption with increasing BFA content observed with some of the EBFABs as shown in Table 3 is a function of the barrier properties of BFA inhibiting water permeation into the epoxy matrix. According to previous studies, the prevailing barrier mechanisms in play here are moisture immobilization by the hydrophilic surface of the BFA and formation of tortuous path by hydrophobic BFA constituents within the epoxy matrix. Another reason for less water uptake could be credited to the BFA-induced increasing crystallinity in the biocomposites. Crystalline regions are impermeable; hence the water absorption is less in such biocomposites [32].

For the NE, surface topology and resin polarity are the primary factors responsible for its moisture uptake despite its hydrophobicity. Soles and Yee in one of their investigations on diffusion of water into epoxy found that water can traverse epoxy network through a network of nanopores that is inherent in epoxy structure [33].

In the present study, three different mechanisms of water absorption/desorption behaviour after saturated mass uptake were identified (Table 3). In case I, the mass uptake index of absorption was greater than the particle dislodgment index, thus, the material continued to absorb water even after saturation mass uptake (material continues to swell). In case II, the mass uptake index of absorption was lower than the particle dislodgement index, hence, the material continued to lose particles into the water which eventually dissolved in the water. After saturation moisture uptake, the material experienced reduction in weight and desorption (material shrinks after swelling). In case III, the mass uptake index of absorption was equal to the particle dislodgement index (counterbalance effect) after saturated moisture uptake, the weight of the material seems constant (materials remain swollen with no appreciable weight gain).

Kinetics of Sorption

From previous research findings, it has been shown that water diffusion into BFPMCs can be

studied via Fick's diffusion model. The model is also used to establish the kinetics of water sorption exhibited by these PMCs.

Table 3. Mechanisms of water absortion/desorption after saturated mass uptake for the NE and the EBFABs.

Samples	Absorption/Desorption Mechanisms after M_∞
10, 15 and 20 wt.% EBFABs	Case I (P_{deb} < Weight Gain by A_{bs})
2, 4 and 6 wt.% EBFABs	Case II (P_{deb} > Weight Gain by A_{bs})
NE and 8 wt.% EBFAB	Case III (P_{deb} = Weight Gain by A_{bs})
*A_{bs} = Absorption and P_{deb} = Particle Deboning	

In general, there are three types of transport phenomena involved in the diffusion of water into PMCs and they are determined by the value of the diffusion exponent (n).

According to the relative rates of diffusion, penetration mobilty and polymer segment relaxation, all cases of diffusion can be distinguished. For a planar geometry the value of n = 0.5 indicates a Fickian diffuision (Case I transport) where the rate of diffusion is smaller than the rate of polymer segment relaxation. For Case II transport, the value of n = 1 where the diffusion process is faster than the polymer segment relxation process. For cases where 0.5 < n < 1, this is regarded as anomalous or non Fickian diffusion where rates of diffusion and polymer segment relaxtion are comparable. Sometimes, when n > 1, it is as regarded as Super Case II Kinetics. And in cases where n < 0.5, this is regarded less Fickian diffusion where the rate of penetration mobility is much below the rate of polymer segment relaxation [34].

**Table 4.** Relationship between water transport phenomena, diffusion exponent and time dependence.

Type of Transport	Diffusion exponent (n)	Time dependence
Less Fickian diffusion	n < 0.5	
Fickian diffusion	n = 0.5	$t^{1/2}$
Non-Fickian (anomalous) diffusion	0.5 < n < 1	t^{n-1}
Case II Transport	n = 1	time independent
Super Case II Kinetics	n > 1	

However, the dominant mechanism is dependent on factors such as filler geometry and morphology, chemical structure of the polymer

and strength and intermellar thickness of interfacial adhesion between filler and matrix [32]. The relationship between the diffusion exponent, type of transport and time dependence is presented in Table 4.

A representative sample of the diffusion fitting curve from which the values of n and k were calculated for the NE and the EBFABs is presented in Fig. 10.
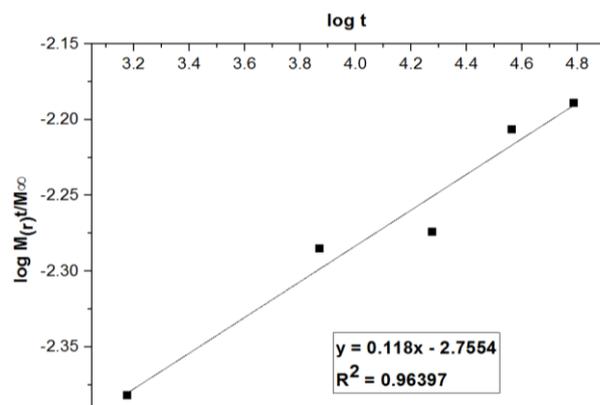
Fig. 10. Diffusion fitting curve for the 15 wt.% EBFAB selected as the representative sample.

Table 5. Values of n and k for the NE and the EBFABs.

| Eq.	y = a + b*x			
Plot	Intercept (k)	Slope (n)	Pearson's (r)	R-Square (COD)
NE	-3.12031 ± 0.2283	0.39294 ± 0.05469	0.97215	0.94508
2 wt.% EBFAB	-2.63672 ± 0.64403	0.31427 ± 0.15428	0.76183	0.58038
4 wt.% EBFAB	-3.66292 ± 0.58298	0.47372 ± 0.13965	0.89061	0.79319
6 wt.% EBFAB	-1.84623 ± 0.52467	0.009579 ± 0.12569	0.40274	0.1622
8 wt.% EBFAB	-2.55718 ± 0.24829	0.26602 ± 0.05948	0.93251	0.86958
10 wt.% EBFAB	-2.59461 ± 0.25621	0.17814 ± 0.06138	0.85872	0.73741
15 wt.% EBFAB	-2.75535 ± 0.05498	0.118 ± 0.01317	0.98182	0.96397
20 wt.% EBFAB	-3.68448 ± 0.09645	0.25596 ± 0.02311	0.988	0.97614

In Table 5, the n and k values of the NE and the EBFABs obtained from diffusion fitting curves using least square method are presented. From

the result, the n values of the EBFABs range between 0.118 ± 0.01317 and 0.47372 ± 0.13965. From the result, only the NE, the 2 wt.% EBFAB and the 4 and wt.% EBFAB have n values that are close to 0.5 which implies that their diffusion mechanisms can be fairly regarded as Fickian. All the other EBFABs exhibited less Fickian diffusion. Also, as revealed by the result, the k values of the EBFABs range between -3.68448 ± 0.09645 and -1.84623 ± 0.52467.

The degree of linearity of the diffusion fitting curves were also evaluated by checking the closeness of the Pearson's r and R-COD square to 1. The NE, the 15 wt.% EBFAB and the 20 wt.% EBFAB exhibited the highest degrees of linearity.

3.7 Biocorrosion

The variation of change in weight with wt.% BFA for the NE and the EBFABs is presented in Fig. 11. The result showed that irrespective of filler content, there was no appreciable change in initial and final weights of the NE and the EBFABs. This is expected for the NE as most synthetic polymers are not microbially biodegradable. The only glaring change in weight (weight gain) was observed with the 8 wt.% EBFAB which is credited to soil moisture uptake. This is also supported by the superlative mass uptake exhibited by this biocomposite as shown in Fig. 9.
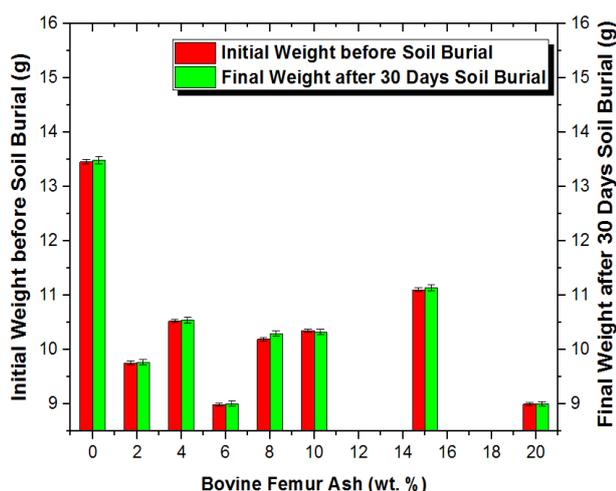
Fig. 11. Variation of weight change with wt.% BFA for the NE and the EBFABs.

Correspondingly, the EBFABs did not biodegrade owing to the absence of microbially degradable collagen fibres in the BFA (completely burnt off during calcination). Collagen fibres are the basic part of skeletons that are highly susceptible to chemical and microbial degradations [35]. This translates to a huge possibility of employing the EBFABs for long-term underground encapsulating applications. However, if the objective is to make synthetic epoxy biodegradable, starches, chitins and keratins have been found by researchers to be highly effective in initiating biodegradation in synthetic polymers [36,37].

4. CONCLUSIONS

The influence of varying volume fractions of micro-sized BFA on the abrasive wear resistance, mechanical behaviour, water transport phenomena and biodegrdation of EBFABs was presented and investigated.

From the research findings, it was observed that the additon of micro-sized BFA to epoxy resin can signinficantly improve its wear, tensile, flexural and water absorbent properties. Also, the ash additon to epoxy did not have any negative influence on the its dimensional stability inside the soil (they are not microbially biodegradable).

It was also observed that enhancement of the investigated properties cut across different volume fractions of the ash. This atypical occurence may be due to mechanical heterogenity of BFA and variations in their localized concentrations within the epoxy matrix. The superlative enhancements in properties with respect to wt.% BFA are given below:

- the 20 wt.% EBFAB gave the superlative enhancement in wear properties;
- the 15 wt.% EBFAB gave the superlative enhancement in tensile modulus;
- the 8 wt.% EBFAB gave the superlative enhancements in tensile and yield strengths;
- the 6 wt.% EBFAB gave the superlative enhancements in flexural strengths at peak and at yield;
- the 4 wt.% gave the superlative enhancement in resistance to water absorption;
- and the 2 wt.% EBFAB gave the superlative enhancement in strain to fracture.

Nonetheless, of all the EBFABs, only the 6 wt.% EBFAB exhibited the optimum combination of the investigated properties.

Suggested areas of applications for the developed EBFABs include but not limited to flooring panels, skateboards, snowboards, keels of yachts and speeding boats, Boeing jets and helicopters support structures, light weight bicycle frames and encapsulants for underground electronic appliances.

REFERENCES

[1] K. Kanimozhi, K. Sethuraman, V. Selvaraj and M. Alagar, 'Development of rice husk ash reinforced bismaleimide toughened epoxy nanocomposites', *Frontiers in Chemistry.*, vol. 2, p. 65, 2014.

[2] R. Nithya and N.M. Sundaram, 'Biodegradation and cytotoxicity of ciprofloxacin-loaded hydroxyapatite-polycaprolactone nanocomposite film for sustainable bone implants', *International Journal of Nanomedicine.*, vol. 10, no. 1, pp. 119, 2015.

[3] S.O. Adeosun, E.I. Akpan and H.A. Akanegbu, 'Thermo-mechanical properties of unsaturated polyester reinforced with coconut and snail shells', *International Journal of Composite Materials*, vol. 5, no. 3, pp. 52-64, 2015.

[4] F. Asuke, M. Abdulwahab, V.S. Aigbodion, O.S. Fayomi and O. Aponbiede, 'Effect of load on the wear behaviour of polypropylene/carbonized bone ash particulate composite', *Egyptian Journal of Basic and Applied Sciences*, vol. 1, no. 1, pp. 67-70, 2014.

[5] I.O. Oladele, J.L. Olajide and Amujede M, 'Wear resistance and mechanical behaviour of epoxy/mollusk shell biocomposites developed for structural applications', *Tribology in Industry*, vol. 38, no. 3, pp. 347-360, 2016.

[6] S. Sekar, A. Mandal, R. Manikandan, S. Sankar and T.P. Sastry, 'Synthesis and characterization of synthetic and natural nano hydroxyapatite composites containing poloxamer coated demineralized bone matrix as bone graft material: a comparative study', *International Journal of Polymeric Materials and Polymeric Biomaterials*, vol. 64, no. 10, pp. 534-40, 2015.

[7] G.S. Kumar, L. Sathish, R. Govindan and E.K. Girija, 'Utilization of snail shells to synthezise hydroxyapatite nanorods for orthopedic applications', *RSC Advances*, vol. 5, no. 49, pp. 39544-8, 2015.

[8] A.A. Nodeh, 'Influence of bone porcelain scraps on the physical characteristics and phase composition of a hard porcelain body', *Boletín de la Sociedad Española de Cerámica y Vidrio*, vol. 56, no. 3, pp. 113-118, 2017.

[9] F.A. Sheikh, M.A. Kanjwal, J. Macossay, M.A. Muhammad, T. Cantu, I.S. Chronakis, N.A. Barakat NA and H.Y. Kim, 'Fabrication of mineralized collagen from bovine waste materials by hydrothermal method as promised biomaterials', *Journal of Biomaterials and Tissue Engineering*, vol. 1, no. 2, pp. 194-7, 2011.

[10] C.C. Pizzolante, J.E. Moraes, S.K. Kakimoto, F.E. Budiño, C. Móri, D.F. Soares and A.P. Saccomani, 'Bovine meat and bone meal as an economically viable alternative in quail feeding in the final phase', *Revista Brasileira de Ciência Avícola*, 18(SPE), pp. 7-12, 2016.

[11] A.S. Jeng, T.K. Haraldsen, A. Grønlund and P.A. Pedersen, 'Meat and bone meal as nitrogen and phosphorus fertilizer to cereals and rye grass', *In Advances in Integrated Soil Fertility Management in sub-Saharan Africa: Challenges and Opportunities*, Springer Netherlands, pp. 245-253, 2007.

[12] B. Jansen, C. Hilmes and D. Jung, 'Bovine spongiform encephalopathy and foot-and-mouth disease, Two animal epidemics transferable to humans. Implications for occupational safety and measures adopted in Germany', *Central European Journal of Occupational and Environmental Medicine Hungary*, 2001.

[13] S.L. Ezeoha and B.O. Ugwuishiwu, 'Status of abattoir wastes research in Nigeria', *Nigerian Journal of Technology*, vol. 30, no. 2, pp. 143-148, 2011.

[14] J.O. Agunsoye, S.I. Talabi, O. Awe and H. Kelechi, 'Mechanical properties and tribological behaviour of recycled polyethylene/cow bone particulate composite', *Journal of Materials Science Research*, vol. 2, no. 2, pp. 41, 2013.

[15] M. Afolabi, O.K. Abubakre, S.A. Lawal and A. Raji, 'Experimental investigation of palm kernel shell and cow bone reinforced polymer composites for brake pad production', *International Journal of Chemistry and Materials Research*, vol. 3, no. 2, pp. 27-40, 2015.

[16] P. Mohan, 'A critical review: the modification, properties, and applications of epoxy resins', *Polymer-Plastics Technology and Engineering*, vol. 52, no. 2, pp. 107-25, 2013.

[17] S.A. Bello, J.O. Agunsoye, S.B. Hassan, M.G. Zebase Kana and I.A. Raheem, 'Epoxy resin based composites, mechanical and tribological

properties: A review', *Tribology in Industry*, vol. 37, no. 4, pp. 500-524, 2015.

[18] S. Husseinsyah, A.N. Azmin and H. Ismail, 'Effect of maleic anhydride-grafted-polyethylene (MAPE) and silane on properties of recycled polyethylene/chitosan biocomposites', *Polymer-Plastics Technology and Engineering,* vol. 52, no. 2, pp. 168-74, 2013.

[19] ASTM D4060-14: *Standard Test Method for Abrasion Resistance of Organic Coatings by the Taber Abraser.* ASTM International, West Conshohocken, PA, ASTM 2014.

[20] ASTM D638-14: *Standard Test Method for Tensile Properties of Plastics*. ASTM International, West Conshohocken, PA, ASTM 2014.

[21] ASTM D790-15e2: *Standard Test Methods for Flexural Properties of Unreinforced and Reinforced Plastics and Electrical Insulating Materials.* ASTM International, West Conshohocken, PA, ASTM 2015.

[22] ASTM D1822-13: *Standard Test Method for Tensile-Impact Energy to Break Plastics and Electrical Insulating Materials*. ASTM International, West Conshohocken, PA, ASTM 2013.

[23] ASTM D570-98e1: *Standard Test Method for Water Absorption of Plastics*. ASTM International, West Conshohocken, PA, ASTM 2010.

[24] M. Gierszewska-Drużyńska and J. Ostrowska-Czubenko, 'Mechanism of water diffusion into noncrosslinked and ionically crosslinked chitosan membranes', *Progress on Chemistry and Application of Chitin and its Derivatives*, vol. 17, pp. 59-66, 2012.

[25] N. Lucas, C. Bienaime, C. Belloy, M. Queneudec, F. Silvestre and J.E. Nava-Saucedo, 'Polymer biodegradation: Mechanisms and estimation techniques–A review', *Chemosphere*, vol. 73, no. 4, pp. 429-42, 2008.

[26] E. Hosseinzadeh, M. Davarpanah, N.H. Nemati and S.A. Tavakoli, 'Fabrication of a hard tissue replacement using natural hydroxyapatite derived from bovine bones by thermal decomposition method', *International Journal of Organ Transplantation Medicine*, vol. 5, no. 1, pp. 23, 2014.

[27] W. Habraken, P. Habibovic, M. Epple and M. Bohner, 'Calcium phosphates in biomedical applications: materials for the future?', *Materials Today*, vol. 19, no. 2, pp. 69-87, 2016.

[28] S. Nobakhti, O.L. Katsamenis, N. Zaarour, G. Limbert and P.J Thurner, 'Elastic modulus varies along the bovine femur', *Journal of the Mechanical Behavior of Biomedical Materials,* vol. 71, pp. 279-85, 2017.

[29] W.D. Callister Jr and D.G. Rethwisch, Fundamentals of Materials Science and Engineering: An integrated approach. New York: John Wiley & Sons, 2012.

[30] K. Ito, M. Kasajima, Y. Ogawa and T. Ojima, 'Microscopic composite mechanism on upper and lower yield points of amorphous polymer solids', *Fibre Science and Technology,* vol. 8, no. 3, pp. 165-72, 1975.

[31] M.R. Zakaria, M.H. Abdul Kudus, H. Md Akil and M.H Zamri, 'Improvement of fracture toughness in epoxy nanocomposites through chemical hybridization of carbon nanotubes and alumina', *Materials*, vol. 10, no. 3, pp. 301, 2017.

[32] M.Z. Abdullah and P.S. Megat-Yusoff, 'Water absorption properties and morphology of polypropylene/polycarbonate/polypropylene-graft-maleic anhydride blends', *Asian Journal of Scientific Research*, vol. 6, no. 2, pp. 167-76, 2013.

[33] C.L. Soles and A.F. Yee, 'A discussion of the molecular mechanisms of moisture transport in epoxy resins', *Journal of Polymer Science Part B: Polymer Physics*, vol. 38, no. 5, pp. 792-802, 2000.

[34] L. Masaro and X.X. Zhu, 'Physical models of diffusion for polymer solutions, gels and solids', *Progress in Polymer Science*, vol. 24, no. 5, pp. 731-75, 1999.

[35] G. Turner-Walker, 'The chemical and microbial degradation of bones and teeth', *Advances in Human Palaeopathology*, pp. 3-29, 2008.

[36] T.F. Garrison, A. Murawski and R.L. Quirino, 'Bio-based polymers with potential for biodegradability', *Polymers,* vol. 8, no. 7, pp. 262, 2016.

[37] A.N. Malathi, K.S. Santhosh and U. Nidoni, 'Recent trends of biodegradable polymer: biodegradable films for food packaging and application of nanotechnology in biodegradable food packaging', *Current Trends in Technology and Science*, vol. 3, no. 2, pp. 73-9, 2014.